Flow enhancement of water-soluble polymers through porous media by preshearing

Yegane, Mohsen Mirzaie; Schmidt, Julia; Dugonjic-Bilic, Fatima; Gerlach, Benjamin; Boukany, Pouyan E.; Zitha, Pacelli L.J.

DOI
10.1021/acs.iecr.1c00099

Publication date
2021

Document Version
Accepted author manuscript

Published in
Industrial and Engineering Chemistry Research

Flow Enhancement of Water-Soluble Polymers Through Porous Media by Pre-shearing

Mohsen Mirzaie Yegane,*[1] Julia Schmidt,[1] Fatima Dugonjic-Bilic,[2] Benjamin Gerlach,[2] Pouyan E. Boukany[3] and Pacelli L. J. Zitha[1]

[1]Department of Geoscience and Engineering, Delft University of Technology, Stevinweg 1, 2628 CN Delft, The Netherlands. E-mail: M.mirzaieyegane@tudelft.nl, P.l.j.zitha@tudelft.nl

[2]TouGas Oilfield Solutions, Weismüllerstraße 50, 60314 Frankfurt am Main, Germany

[3]Department of Chemical Engineering, Delft University of Technology, Van der Maasweg 9, 2629 HZ Delft, The Netherlands

KEYWORDS: Polymer, rheology, pre-shearing, porous media, flow efficiency, chemical enhanced oil recovery (cEOR)

ABSTRACT: We examine the role of pre-shearing on the flow properties of polymer solutions containing essentially an acrylamide-based copolymer obtained from an emulsified polymer emulsion inverted by a surfactant. The polymer solutions were pre-sheared using three methods: (1) a Buddeberg disperser (2) an Ultra-Turrax disperser and (3) pressure-driven flow through a capillary. Shearing the polymer solution was done under fast flow to induce high-stretching of the polymer chains and thus promote the break-up of the longest ones (i.e. decrease in relaxation time and shear-thinning level). The un-sheared and pre-sheared polymer solutions were forced through sand-packs to compare their corresponding flow resistances. We observed that the reduction in the viscosity and screen factor of the pre-sheared polymer solutions is path independent regardless of the shearing device. We found a critical Weissenberg number (Wi_c~13) above which the viscosity of the polymer solutions started to decrease. The resistance factor for the polymer solutions pre-sheared with the Ultra-Turrax disperser at an energy input of 31.3 MJ/m^3 and 290.7 MJ/m^3 was nearly 3 and 7 times respectively lower than for the un-sheared polymer solution, while the viscosity decreased only by 27% and 48% respectively. The sand-pack experiments were successfully interpreted using a numerical model taking into account time-dependent retention. The model showed that the flow of the pre-sheared polymer solutions through the sand-packs was enhanced mainly due to breaking the longest polymer chains, which results in smaller mechanical entrapment. This pre-shearing of the water-soluble polymers can be used in multiple industrial applications including chemical enhanced oil recovery and optimization of polymer processing.

1. INTRODUCTION

Long polymer chains can break due to strong flow-induced chain scission. This can be undesirable in many practical applications including turbulent drag reduction of dilute solutions of high molecular weight polymers[1] or polymer/DNA characterization methods such as high shear rheology in microfluidics[2-4] and gel permeation chromatography (GPC). However, if done in a controlled manner, chain scission can be desirable in other applications. Examples include drug delivery[5, 6], lithography[7, 8], and chemical enhanced oil recovery (cEOR)[9], to mention only a few.

In cEOR applications, the addition of polymers aims at viscosifying the water. Controlled chain scission of polymers (often referred to as controlled pre-shearing) has been used to improve their flow efficiency in porous media i.e. to reduce the flow resistance.[10-12] Polymers used in cEOR typically have a large size and are polydisperse, i.e. have a broad molecular weight distribution (MWD).[11] Long polymer chains offer more flow resistance and tend to block the smallest pores in porous media leading to a time-dependent injectivity decline.[13-15] The premise of the controlled pre-shearing is to (a) stretch all the polymer chains and (b) break the longest polymer chains into smaller size chains by strong flow-induced chain scission[16], as will be discussed in more detail below. The latter includes the homolytic scission of valence bonds, which connects the atoms to form the macromolecule.[17]

Pre-shearing of polymer solutions in dilute and semi-dilute regimes was investigated by several authors building upon the work of De Gennes.[18] This work predicted that random polymer coiled in dilute solutions will be fully extended due to a coil–stretch transition at a critical strain rate ($\dot{\varepsilon}_c$). This strain rate is larger than the rate of relaxation ($\frac{1}{\lambda}$ where λ is the longest relaxation time of the polymer chain). This is equivalent to the Weissenberg number (Wi), defined as the product of strain rate and relaxation time, larger than 1. Theoretical calculation based on the Zimm model[19] and numerical calculation by Larson and Magda[20] indicated that the onset of the coil–stretch transition takes place when Wi > 0.5. Later, single molecule experiments (based on DNA visualization) were combined with microfluidic devices to confirm the onset of the coil–stretch transition during flow at Wi > 0.5.[21-23] Odell et al.[24]

predicated the mid-chain scission occurs due to a continuous increase of stress on the center of the chain when the strain rate is larger than a critical strain rate known as a critical fracture ($\dot{\varepsilon_f}$). Since the relaxation time increases with chain length[25], for a polydisperse polymer, Wi for the longest chains is larger than for the shortest chains. Hence, the longer chains are more prone to mid-chain scission than the smaller ones. This implies that first, at a certain critical strain rate ($\dot{\varepsilon_{fl}}$), the longer polymer chains are broken and consequently, at a higher critical strain rate ($\dot{\varepsilon_{fs}}$), the shorter chains are broken. It was experimentally shown that mid-chain scission is induced by elongational flow field[26, 27] as well as ultrasonic cavitation.[28, 29] On the other hand, pre-shearing a polymer solution in semi-dilute regime is concentration dependent.[30] Unlike the dilute regime for which the mid-chain scission occurs, in the semi-dilute regime the chain scission is increasingly randomized at higher concentrations.[31]

Several studies have investigated rheological properties of sheared polymer solutions[24, 31], and their flow behavior in contractions.[30, 32] They found that shearing the water-soluble polymers, such as hydrolyzed polyacrylamide (HPAM) and polyethylene oxide (PEO), improve their flow efficiency in contractions. However, the behavior of pre-sheared polymer solutions in porous media remains poorly understood, which demands a detailed study that links the rheology of pre-sheared water-soluble polymers to their porous media flow characteristics.

In this study, we investigate the porous media flow enhancement of polymer solutions by controlled pre-shearing. The polymer solutions contained an acrylamide-based copolymer obtained by inversion of an emulsified polymer emulsion. The pre-shearing was achieved using two agitators (a Buddeberg disperser and an Ultra-Turrax disperser) and pressure-driven flow through capillaries. The pre-shearing was done at various shearing intensities, equivalent to different strain rates. To ensure the reduction of the porous media flow resistance while maintaining the viscosity, the applied strain rates were higher than $\dot{\varepsilon_c}$ and $\dot{\varepsilon_{fl}}$ but smaller than $\dot{\varepsilon_{fs}}$. A detailed rheological analysis was carried out to examine the response of pre-shearing on the polymer solutions for each shearing device. The viscosity, screen factor, and imposed energy input by pre-shearing were determined, which allows for studying the dependencies and correlations between the rheological parameters. Based on the rheological experiments, sand-pack flow experiments were conducted. The porous media flow behavior for differently pre-sheared polymer solutions was studied by observing dependencies between these tests and rheological experiments. Moreover, a numerical simulation based on a one-dimensional model was developed aiming at studying the mechanisms of flow efficiency in porous media.

2. EXPERIMENTAL

2.1. Materials. The polymer solution used to conduct the experiments, designated as PS-A, contained essentially an acrylamide-based copolymer. PS-A was obtained from an active emulsion polymer (designated as EP-A) which was inverted by an active inverter surfactant (designated as IS-A). PS-A contained 0.4 wt% EP-A and 0.24 wt% IS-A (1 wt% ~ 10,000 ppm). The molecular weight of the polymer (Mw) was estimated to be around 2.5×10^6 g/mol (see Section 4 in the supporting information). The solvent was synthetic seawater SSW-A having total dissolved solids (TDS) of approximately 5 wt%. The exact composition of SSW-A is given in Table 1. Detail of a typical inverse polymerization to synthesize acrylamide-based polymers is described elsewhere.[33, 34] Here, we highlight only the important aspects and focus on the role of pre-shearing on the flow response of polymer solutions. PS-A was prepared by first adding IS-A to SSW-A, followed by the addition of EP-A under continuous mixing with a magnetic stirrer set to 600 revolutions per minute (rpm) at room temperature. The polymer system was fully inverted after a few minutes of gentle stirring, yet to ensure that all polymer chains were released, the solution was stirred for an additional 45 min. No viscosity loss occurred as proven by measuring the viscosity at different stirring times. The obtained polymer solution is referred to as the un-sheared polymer solution. The critical overlap concentration of the polymer was found to be 0.40 ± 0.01 wt% (see Figure S3 in the supporting information). This indicates that the selected concentration of polymer in PS-A is close to the overlap concentration.

2.2. Polymer Pre-Shearing. Polymer solutions obtained as described above were pre-sheared using three different shearing devices. Two agitators were used, namely, a Buddeberg DS5 disperser (hereafter referred to as Buddeberg), and an Ultra-Turrax S25 N-18G disperser (hereafter referred to as Ultra-Turrax) to shear the polymer solution at various intensities The polymer solution was sheared in Buddeberg using a toothed circular disk stirrer and in Ultra-Turrax by forcing the solution through the gaps of the rotating rotor in the shear gap between the rotor and stator. In the third method, the polymer solution was sheared by forcing it through a capillary die. This set-up consists of a steel cylinder with a volume of 300 mL and an attached capillary with an inner diameter of 1 mm and varying lengths of 3, 10, and 20 cm at the end of the cylinder. At the top of the cylinder, pressures between 1 to 20 bar were applied using compressed air. 250 mL of inverted polymer solution was filled in the cylinder and forced through the capillary at a constant pressure drop. At the exit of the capillary, the extruded polymer solution was collected in a beaker placed on a balance to estimate the volumetric flow.

A summary of pre-shearing the polymer solutions at different shearing intensities for Buddeberg and Ultra-Turrax or different applied pressures for capillary is given in Table 2 which were translated to volume specific energy input and Weissenberg number (see Sections 2 and 3 in the supporting information for more details). As mentioned, pre-shearing the polymer solution promotes stretching the polymer chains (equivalent to increasing Wi, see Figure 1a) and breaking the longest ones. In literature, the latter is attributed to breaking the high molecular weight fragments of MWD into lower molecular weight fragments resulting in a narrower MWD (see Figure 1b).[16, 35]

Table 1. The synthetic Seawater SSW-A composition with ~ 5 wt% TDS (1 wt% ~ 10,000 ppm)

Component	Na^+	K^+	Mg^{2+}	Ca^{2+}	Sr^{2+}	Cl^-	$SO4^{2-}$	HCO^{3-}	TDS
Concentration (ppm)	151,121	511	1,928	649	3	27,771	3,700	153	49,836

Table 2. The shearing intensities or applied pressures for each shearing device

Shearing device	Shearing intensity (rotational speed or pressure drop)	Shearing duration or length of the capillary
Buddeberg	500, 750, 1000, 1250, 1500 and 1750 rpm	30 and 60 min
Ultra-Turrax	5,000, 10,000, and 20,000 rpm	1, 3.25, 5, 7.75, and 10 min
Capillary	1, 2, 3, 4, 5, 10, and 20 bar	3, 10 and 20 cm

2.3. Rheological Measurements. To study the role of the shearing devices on the flow properties of the polymer solutions, we have performed a rheological analysis on the polymer solutions (before and after pre-shearing). The viscosity of the polymer solutions (η) was determined by an Ubbelohde viscometer (type number 501 13 Ic). The screen factor (SF) which is a measure of the elongational viscosity from stretched to the coiled state was determined in a screen viscometer.[36] The screen factor is defined as the time that a certain volume of the polymer solution needs to pass through five 100-mesh screens to the flow time for the same volume of the solvent through the screens.[12] SF measurement has been typically employed to determine whether mechanical degradation of a polymer solution has occurred during a process.[11] The viscosity of the un-sheared polymer solution (η_0) was found to be 12.5 ± 0.6 mPa s and its screen factor (SF_0) was 19.0 ± 0.9.

The viscosity of polymer solutions as a function of shear rate was measured using a commercial rheometer (MCR-302, Anton Paar GmbH) in a Couette cell (cup ID = 28.92 mm, bob OD = 26.66 mm, gap = 1.18 mm). To study the shear-thinning behavior of the polymer solutions, Carreau–Yasuda model[37] as shown below was used:

$$\eta - \eta_\infty = (\eta_\mathrm{i} - \eta_\infty)[1 + (\dot{\gamma}\lambda)^a]^{\frac{n-1}{a}} \qquad (1)$$

where η is the shear dependent polymer viscosity, η_∞ is assumed to be the solvent viscosity, η_i is the zero shear rate viscosity, $\dot{\gamma}$ is the shear rate and λ is the relaxation time which is the inverse of a critical shear rate where the transition from Newtonian to shear-thinning occurs. Here, the parameter n is the power-law exponent obtained from the shear-thinning part and allows controlling over the width of the transition region from Newtonian to shear-thinning.

The amplitude sweep was also performed and the storage and loss moduli were measured as a function of strain. All the rheological measurements in this study were performed at 30 °C.

2.4. Sand-Pack Flow Experiments. A sand-pack was used as the model porous medium: 20.0 ± 0.1 g of quartz sand (99 pure quartz with trace quantities of iron oxide) having grain sizes smaller than 125 µm was packed in a cylindrical cell with inner diameter and length of 1.52 and 7.50 cm respectively. At the bottom of the sand cell, a 30 µm square mesh filter and a coarser filter were installed. The sand was fitted into the sand cell under continuous gentle hammering in the vertical and horizontal directions. The pore volume (PV) and porosity of the sand-pack were found to be 6.5 ± 0.1 mL and 46 ± 1% respectively. Before the flow test, the sand-pack cell was evacuated and then flushed with SSW-A for 10 min.

Figure 1c presents the schematic of the sand-pack flow set-up that was designed to conduct the experiments. A pressure sensor type A-10 from WIKA with a measurement range of 0 to 4 bar and an accuracy of 0.5% was installed on top of the sand-pack cell. SSW-A was pumped either directly into the sand-pack or in an equalizing tank filled with a spacer-oil. The spacer oil displaces the polymer solution in the polymer tank, which allows the polymer solution to flow in the sand-pack cell without being directly pumped. This ensures that no mechanical degradation of the polymer occurs by pumping.

2.5. Sand-Pack Flow Experimental Procedure. The procedure of the sand-pack flow tests is shown in Table 3. The sand-pack was flushed with SSW-A for 30 min at 3 mL/min, which is equivalent to 14.0 ± 0.5 pore volume (PV), to ensure 100% saturation of the sand-pack with SSW-A. After that, the permeability test was performed and the permeability of the sand-pack cell was determined to be 1,000 ± 100 mD. Next, the flow rate was switched from 3 to 0.5 mL/min and the injection continued for another 30 min (equivalent to 2.0 ± 0.5 PV) followed by the polymer injection. The polymer solution was injected for 30.0 ± 0.5 PV. Resistance factor RF (defined as the ratio of the pressure drop of polymer solution over the pressure drop of SSW-A) was monitored for the whole injection cycle (see Section 1 in the supporting information for more details on RF). This was to assess the flow resistance of the polymer solutions.

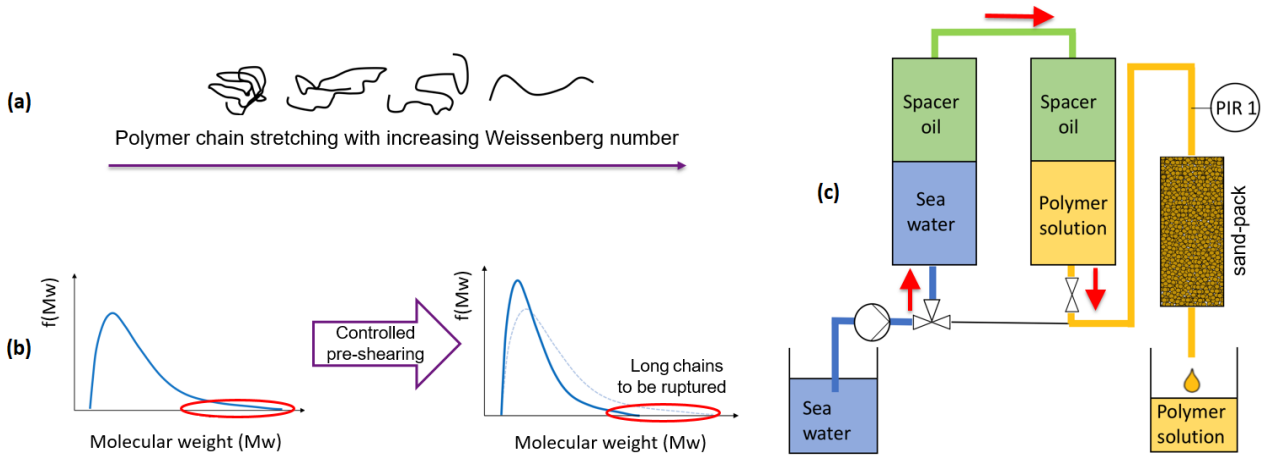

Figure 1. (a) Stretching a polymer chain by increasing Weissenberg number (*Wi*). At Weissenberg numbers higher than 1 the polymer is fully extended due to the coil–stretch transition. (b) Breaking the high-end fragments of the polymer MWD by controlled pre-shearing. The red ellipse highlights the longest chains which have a higher potential to be ruptured. In the molecular weight distribution on the right-hand side, the dashed line represents the original MWD and the solid line represents the MWD for the pre-sheared polymer. (c) Schematic of the flow of the pre-sheared polymer solution through a sand-pack. SSW-A is either directly forced into the sand-pack or is pumped in the first equalizing tank where the spacer oil stays on top. Thereafter, the spacer oil moves to the second equalizing tank and pushes the polymer solution into the sand-pack.[38] Reproduced with permission from ref. 38. Copyright 2019 Society of Petroleum Engineers

Table 3. Overview of sand-pack flow experimental procedure

Sequence	Injected fluid	Injection rate (mL/min)	Injection time (min)	Number of injected pore volumes
1	Synthetic seawater SSW-A	3	30	~14
2	Synthetic seawater SSW-A	0.5	30	~2
3	Polymer solution PS-A	0.5	Overnight	~30

2.6. Sand-Pack Flow Numerical Simulation. The polymer flow efficiency in the sand-packs was also investigated by solving numerically the one-dimensional model for polymer flow in porous media introduced by Yerramilli et al.[39] The model accounts for time-dependent polymer retention in addition to advection, dispersion, filtration, and static adsorption. A custom-made MATLAB code was used to solve the equations. The details and equations used in the model can be found in ref. 39. Figure S6 in the supporting information represents the workflow used for the simulation. Here, we only present key features of the proposed model.

Polymer response to pre-shearing: The effect of pre-shearing the polymer chains was modeled using the conceptual model introduced by Sorbie and Roberts[35] which is based on a discrete multi-component representation of the polymer MWD. The model assumes that during pre-shearing, the MWD changes as higher components degrade into lower molecular weight fragments. Therefore, the average molecular weight ($\overline{Mw}$) of polymers shifts to the left (i.e. lower molecular weight) while the amount of polymers corresponded to this the average molecular weight ($\bar{C}$) shifts upward (i.e. increase in the amount). Sorbie and Roberts[35] proposed the following equations to model the change in MWD because of pre-shearing:

$$\overline{[\eta]} = A(\overline{Mw})^b \qquad (2)$$

$$\bar{\eta} = \eta_s \overline{[\eta]} \bar{C} \qquad (3)$$

where $\bar{\eta}$ and $\overline{[\eta]}$ are the average polymer viscosity and average intrinsic viscosity respectively. b and A equal to 0.87 and 2.6 × 10^{-7} respectively gives $\overline{[\eta]}$ in ppm^{-1} and $\bar{C}$ in ppm.[35] For the un-sheared polymer solution, $\overline{Mw}$ used in the model was obtained using the methodology explained in Section 4 in the supporting information and $\overline{[\eta]}$ and $\bar{C}$ can be calculated using Equations 2 and 3 respectively. For pre-sheared polymer solutions, the average polymer viscosity is already known from the experiments and $\overline{Mw}$ and $\bar{C}$ are used as the matching parameters according to Equations 2 and 3 to obtain the same value of viscosity. The change in $\overline{Mw}$ and $\bar{C}$ is based on the trend explained above (i.e. a decrease in $\overline{Mw}$ and an increase in $\bar{C}$ with increasing energy input). As a result, for each shearing condition $\overline{Mw}$ and $\overline{[\eta]}$ are input to the model.

Polymer viscosity model: The dependence of polymer viscosity on concentration was modeled using the modified Flory–Huggins equation described by Equation 4:

$$\eta_i = \eta_s \left[1 + \left(a_1 c_p + a_1 c_p^2 + a_1 c_p^3\right) S_s^m\right] \qquad (4)$$

where a_1, a_2 and a_3 are the polymer viscosity fitting parameters and vary with the salinity of the solvent (S_s) and m is the slop of $(\eta_i - \eta_s)/\eta_s$ versus S_s on a log-log plot for given energy input.[39] Considering the viscosity values found from experiments, the matching parameters for each

shearing condition are obtained which can be seen in Table S2.

Time-dependent reduction of pore throat radius: To capture the time-dependent pressure behavior observed for the un-sheared model we proposed a simple model where pore throat radius decreases with time. Physically this is equivalent to the formation of an impermeable polymer adsorption layer on the pore walls with a thickness that grows over time. The growth rate of the polymer layer thickness depends on the characteristic size of the polymer molecules in the solution and thus also on the molecular weight. The model considers that pore throat radius reduces with the injection of many pore volumes of the polymer solutions. In this simple model, the polymer retention, as a result of adsorption and mechanical entrapment, increases continuously rather than leveling off to an equilibrium value.

3. RESULTS AND DISCUSSION

3.1. Rheological Response of Pre-Sheared Polymer Chains. To understand the impact of pre-shearing on the polymer performance, the viscosity and screen factor were measured for polymer solutions sheared by Buddeberg, Ultra-Turrax, and the capillary die with different shearing intensities (see Table 2 for details of the shearing conditions with each device). The viscosities were measured with an Ubbelohde viscometer and were converted to zero shear rate viscosity using the correlation explained in Section 7 of the supporting information. Figure 2a-b shows the viscosity and screen factor of Buddeberg sheared PS-A as a function of rotational speed. It was observed that shearing PS-A for 30 and 60 min leads to comparable viscosities and screen factors suggesting that doubling the shearing time had no significant impact on the viscosity reduction. Shearing the polymer solution at a rotational speed of 500 rpm hardly influenced the screen factor suggesting that the applied strain rate was too small to break the polymer chains. However, from this rotational speed onwards, the screen factor decreased continuously. At 1,750 rpm, for instance, the screen factor was reduced by 36%. Furthermore, the viscosity was not substantially affected by shearing irrespective of the rotational speed and it decreased only by 7% after 30 min at 1,750 rpm. A significant difference between the change in screen factor and viscosity indicates that Buddeberg ruptures the high-end fragments of MWD without significantly rupturing the shorter chains.

Figure 2c-d shows that for Ultra-Turrax sheared PS-A at a rotational speed of 5,000 rpm, the screen factor dropped by 29% whereas the viscosity decreased only by 11%. This is identical to what was observed for Buddeberg (i.e. rupturing the high-end fragments of MWD only). However, increasing the rotational speed to 10,000, and 20,000 rpm had a much more significant effect on the viscosity and screen factor; viscosity decreased by 35% and 50% and screen factor dropped by 51% and 71% respectively. It can thus be inferred that shearing the polymer solution at rotational speeds larger than 5,000 rpm makes the strain rate higher than $\dot{\varepsilon}_{fs}$ and decreases viscosity more significantly. Moreover, for each rotational speed, the screen factors asymptotically tend to a final value meaning that after some point the shearing time no longer affects the screen factor. This is consistent with experimental observation for Buddeberg where shearing the polymer solution for an additional 30 min had little effect on the screen factor.

For the capillary sheared polymer solutions, the viscosity and screen factor were measured for capillaries with different lengths at various pressure drops (see Table 2). The total pressure drop across a capillary die is a summation of three contributions: entry pressure drop, end pressure drop, and pressure drop due to the friction of the polymer solution with the wall over the length of the capillary. Entry and end pressure drops are nearly equal for different lengths while the frictional pressure drop increases with the capillary length. Therefore, for a certain pressure drop, degradation is higher in shorter capillaries. To investigate the viscosity and screen factor change as a function of flow rate in capillaries, the pressure drops were translated to equivalent flow rates using the Poiseuille equation. As can be seen in Figure 2e-f, the viscosity and screen factor decreased with the flow rate. This decrease was more pronounced in the shortest capillary (L/r = 60, where L and r represent the length and radius of the capillary die) where the observed viscosity and screen factor losses were 30% and 52% respectively.

Deformation and breaking of the polymer chains is dependent on the type of flow and the chemistry of the polymer [40]. The nature of the flow field created by these shearing devices is complex and differs from one device to another. Using shearing devices with a region of strong extensional flow such as Buddeberg and Ultra-Turrax, the chains may be completely stretched before breaking in their center. [30] In flow through capillaries, however, a large proportion of the chains experience the extensional flow field and rupture before they are fully stretched (this has been reported for polyacrylamide in the turbulent flow and dilute regime[32, 41] which is identical to the condition of our experiments). Moreover, the residence time for flow in the capillary die was shorter than for the flow in Buddeberg and Ultra-Turrax.

To gain a more detailed insight on how the polymer chains are deformed as a result of pre-shearing, the normalized viscosity is plotted as a function of Wi (see Figure 3). Note that the viscosity data reported in Figure 3 for the polymer solution pre-sheared with Ultra-Turrax are after 7.75 min shearing at a rotational speed of 5,000, 10,000, and 20,000 rpm. The relaxation time for the calculation of Wi was obtained from the Carreau–Yasuda model (see Figure 5).

The minimum calculated Wi, for the polymer chains sheared by three shearing devices, was 6 ± 1. This suggests that a coil–stretch transition has occurred even at the lowest rotational speed of the agitators and lowest flow rate of the capillary die in our study. The viscosity of the polymer solutions remained un-changed up to a critical Weissenberg number (Wi_c~13). Then beyond this value, it decreased according to a logarithmic function of Wi. Data in Figure 3 indicates that polymer pre-shearing is path independent, i.e. the viscosity decreases in the same way regardless of the shearing device used for pre-shearing. Moreover, it can be inferred that the rate of viscosity reduction becomes slower at higher Wi (> 60 ± 1). This suggests that once certain stress is applied to the polymer, first, longer polymer chains (higher-end fragments of MWD) are ruptured. To rupture the smaller polymer chains (lower-end fragments of MWD), a

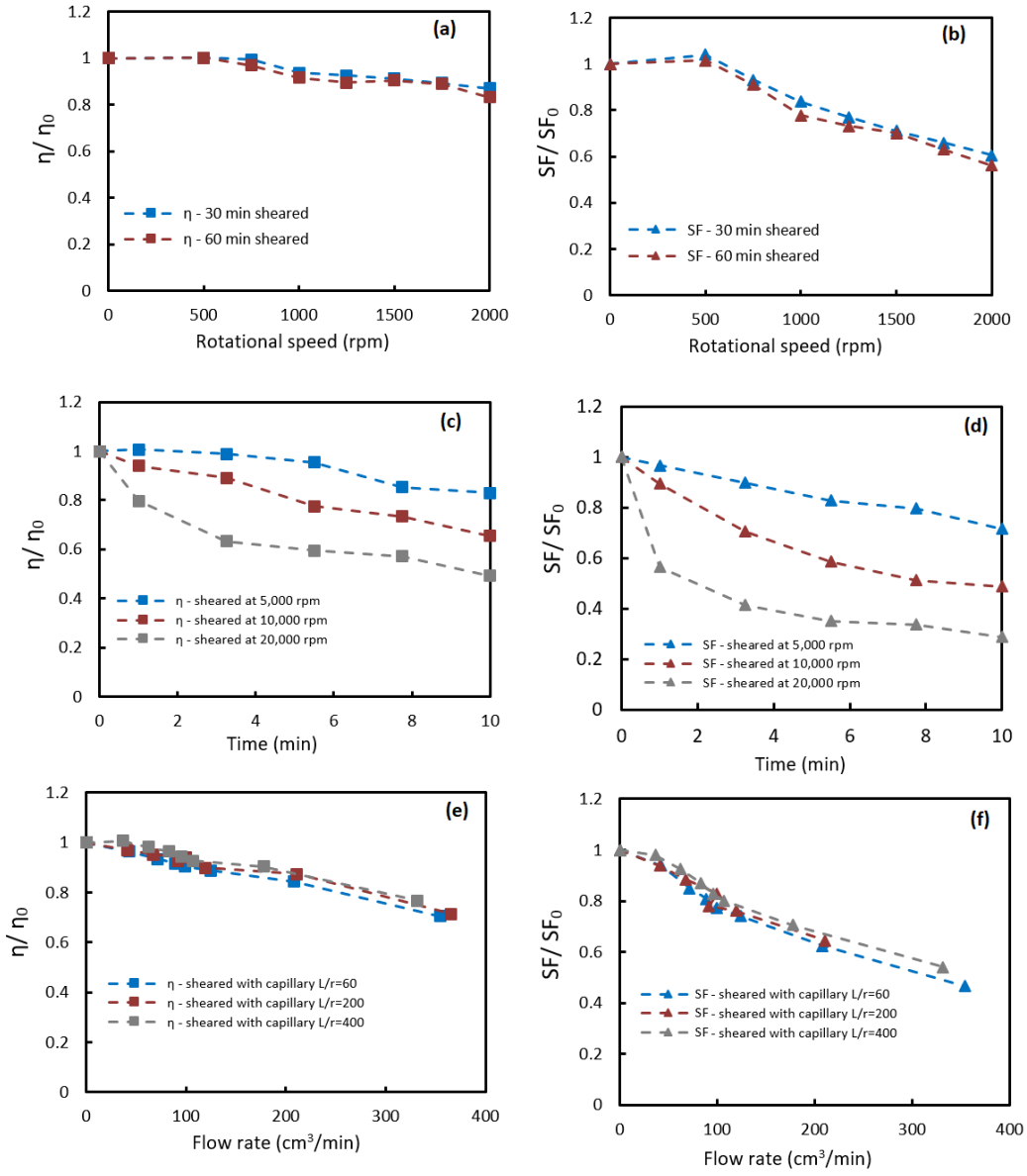

Figure 2. Impact of pre-shearing on the viscosity and screen factor of the polymer solutions. For Buddeberg: (a) the normalized viscosity and (b) the normalized screen factor as a function of rotational speed after 30 and 60 min of shearing. For Ultra-Turrax: (c) the normalized viscosity and (d) the normalized screen factor as a function of shearing time at a rotational speed of 5,000, 10,000, and 20,000 rpm. For capillary: (e) the normalized viscosity and (f) the normalized screen factor as a function of flow rate for L/r ratios of 60, 200 and 400

higher Wi is needed. This is in good agreement with the observation of Odell et al.[24, 42] where the critical strain rate to rupture the chains scales with $1/Mw^2$. Mw for the pre-shared polymer solutions was measured and plotted as a function of Wi (see Figure S4 in the supporting information). The fact that Mw decreases only at Weissenberg numbers higher than Wi_c indicates the rupture of the longest chains at high strain rates. The effect of shearing time on the reduction of the molecular weight for polymer solutions sheared with Ultra-Turrax was also investigated (see Figure S5 in the supporting information). We found that for a certain strain rate there is a critical Mw below which there is no reduction in viscosity. This means that the reduction of Mw as a function of shearing time evolves towards a critical plateau value (Mw_c). Beyond Mw_c, polymer chains can no longer be broken irrespective of the duration of pre-shearing. The value of Wi_c obtained from our study is in good agreement with that obtained by Garrepally et al.[32] who found Wi_c for sheared polymers in the range of 11 to 22 depending on the Mw.

An important remark should be made concerning the calculation of the Weissenberg number. Wi can be used for both shear and extensional flows.[4] For the former, the Weissenberg number is defined as $Wi = \dot{\gamma}\lambda$ and for the latter, it is defined as $Wi = \dot{\varepsilon}\lambda$. The geometries used in this study combine shear and extensional flows. For these types of flow, it is generally accepted that a one-to-one relationship between strain rate and shear rate exists;[43-45] however, the exact form of such relationship may differ from one geometry to another. We calculate the Weissenberg number using $Wi = \dot{\varepsilon}\lambda$ for the capillary die. The Weissenberg number for Buddeberg and Ultra-Turrax, however, was calculated using $Wi = \dot{\gamma}\lambda$ as available analytical expressions only allowed us to convert the rotational speed of these shearing devices to shear rate.

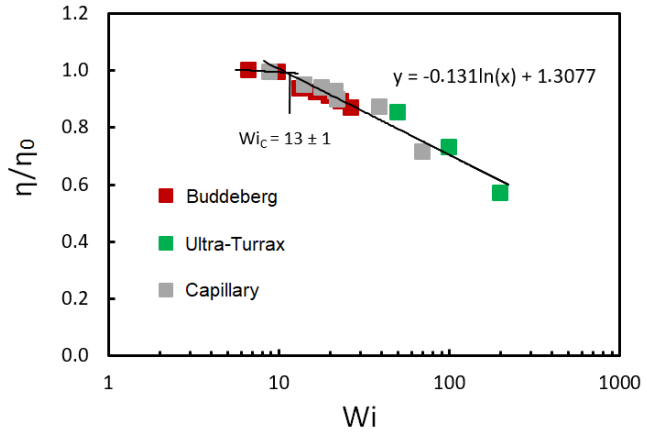

Figure 3. The normalized viscosity versus Weissenberg number. Red, green, and grey data points represent Buddeberg, Ultra-Turrax, and capillary respectively

3.2. Effect of Stored Energy. The impact of pre-shearing on the performance of the polymer solution was further examined by calculating the energy input on polymer chains based on the shearing intensity to reconcile the differences between flow types in the shearing devices. In this approach, the friction and consequent chain stretching and rupturing are not attributed to the strain experienced by the polymer. They are rather related to the total accumulated strain, corresponding to the total energy stored.[30] Degradation results from energy accumulation during the stretching process which is correlated with the energy dissipated by the shearing devices.[40, 46]

The superimposed volume specific energy input by the agitators can be estimated by the turbine-power correlations, which is expressed by power number (N_p) versus Reynolds number for agitators (R_e). For this, the power input (P_N) has to be determined first as follows:[47]

$$P_N = N_p \cdot \rho \cdot n_r^3 \cdot d_i^5 \qquad (5)$$

where ρ is the fluid density, n_r is the rotational speed, and d_i is the diameter of the agitator. N_p is found from the power number-Reynolds number relationship which is known for many agitators. R_e is calculated by Equation 6 in the following way:[47]

$$R_e = \frac{\rho \cdot n_r \cdot d_i^2}{\eta} \qquad (6)$$

The imposed volume specific energy input (E_v) on the polymer solution is then determined by Equation 7:

$$E_v = \frac{P_N \cdot t}{V} \qquad (7)$$

where t is the stirring time, and V is the stirred volume. A more detailed explanation of the calculation of the volume specific energy input is given in Section 2 of the supporting information.

As shown in Figure 4a-b, two master curves could be established for the viscosity/screen factor as a function of volume specific energy input, independent of the shearing device. Both the viscosity and screen factor decreased as the energy input increased. The viscosity decreased as a power-law function and the screen factor decreased as a logarithmic function of energy input.

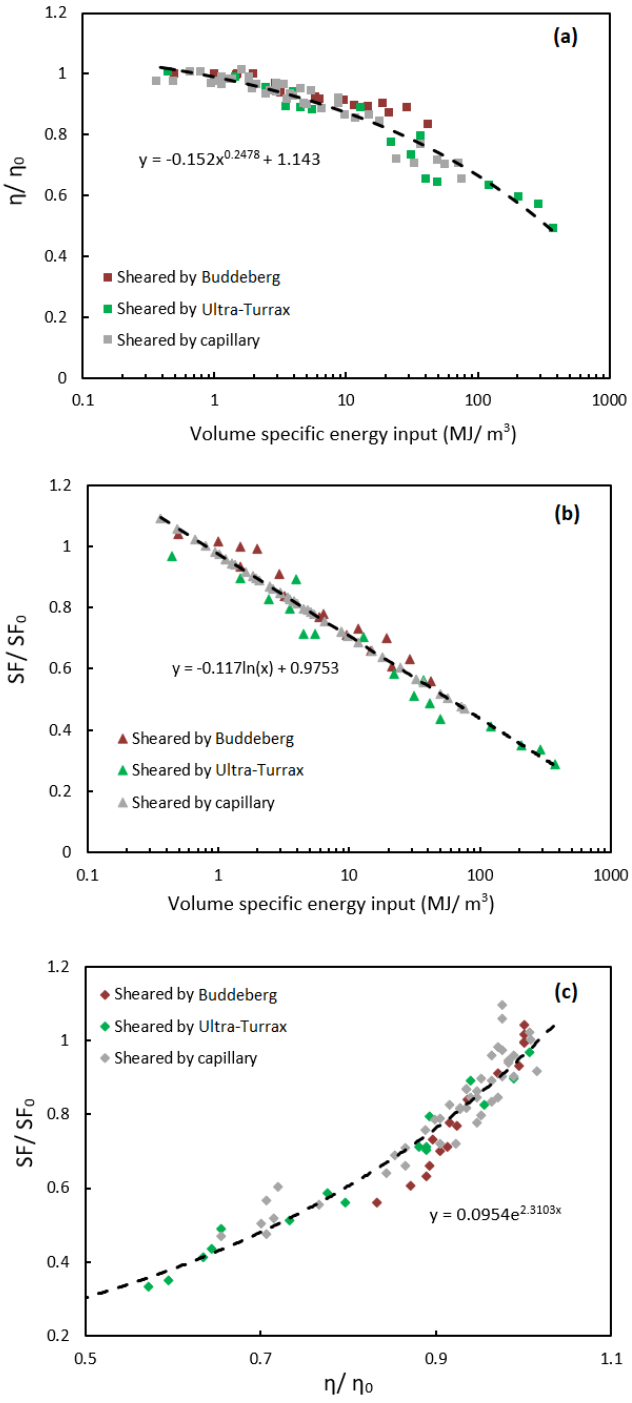

Figure 4. The change in viscosity and screen factor versus shearing intensity (based on the energy input) from the experimental series. (a) The normalized viscosity and (b) the normalized screen factor as a function of energy input and (c) the normalized screen factor as a function of the normalized viscosity. Red, green, and grey data points represent Buddeberg, Ultra-Turrax, and capillary respectively. The data presented here correspond to the data given in Figure 2

As shown in Figure 4c, another master curve was established between the screen factor and viscosity of the pre-sheared polymer solutions independent of the shearing

device. The screen factor increased according to an exponential function of the viscosity. At the beginning of the pre-shearing process, only the screen factor decreased sharply while the reduction in viscosity was not as much. Later, both the screen factor and viscosity decreased significantly. This supports the hypothesis that by shearing the polymer solution, first the long polymer chains are ruptured (i.e. mainly reduction in the screen factor) but after a critical strain rate, shorter polymer chains are ruptured as well (i.e. reduction in both the screen factor and viscosity).

The shear viscosity measurements were performed for PS-A with no pre-shearing and pre-sheared PS-A with Buddeberg, Ultra-Turrax, and capillary at different energy inputs (see Figure 5a). The Carreau–Yasuda model (Equation 1) was used to fit the experimental data. The list of fitting parameters is tabulated in Table S1 (see the supporting information). Data show that regardless of shearing conditions, PS-A exhibits a Newtonian behavior in low to intermediate shear rates followed by a shear-thinning behavior at higher shear rates. The extension of Newtonian and shear-thinning regimes depends on the energy input. The shear rate dependency of PS-A decreased with increasing the energy input. On the other hand, from Table S1 can be seen that relaxation time decreases with increasing energy input. This means that at higher energy input, the polymer solutions contain shorter polymer chains, and chains are more stretched. Consequently, when a polymer molecule is deformed by shear forces, it requires a shorter time to relax to its original conformation.

3.3. Viscoelastic Response of Pre-sheared Polymer Chains. Amplitude sweep tests were conducted to measure the storage modulus (G') and loss modulus (G'') as a function of strain (γ) at a constant angular frequency (ω) of 6.28 rad/s. This test was attempted with PS-A with no pre-shearing and PS-A sheared with Buddeberg and Ultra-Turrax at volume specific energy input of 14.6 and 40.8 MJ/m^3 respectively. As can be seen in Figure 5b, for PS-A with no pre-shearing the loss modulus was larger than the storage modulus over the range of strains up to 1000% implying that even in the absence of pre-shearing the rheological response of the polymer solution is controlled by the viscous component and there is no significant entanglement among the polymer chains. With increasing the energy input imposed by Buddeberg and Ultra-Turrax, both G' and G'' decreased while the response was still completely viscous dominant. This is again an indication of stretching the polymer chains and breaking the longest ones by pre-shearing.

3.4. Effect of Pre-Shearing on Porous Media Flow. Based on the results of the rheology of pre-sheared polymer chains, the following polymer solutions were selected for the sand-pack flow experiments: PS-A with no pre-shearing and Ultra-Turrax sheared PS-A with an energy input of 31.3 MJ/m^3 and 290.7 MJ/m^3. Here, we focus on polymer solutions pre-sheared by the Ultra-Turrax only at different energy inputs, as the flow field is similar and this enables the investigation of the effect of energy input on the flow enhancement due to pre-shearing. The performed sand-pack flow experiments are summarized in Table 4. Results will be discussed and interpreted in terms of the resistance factor

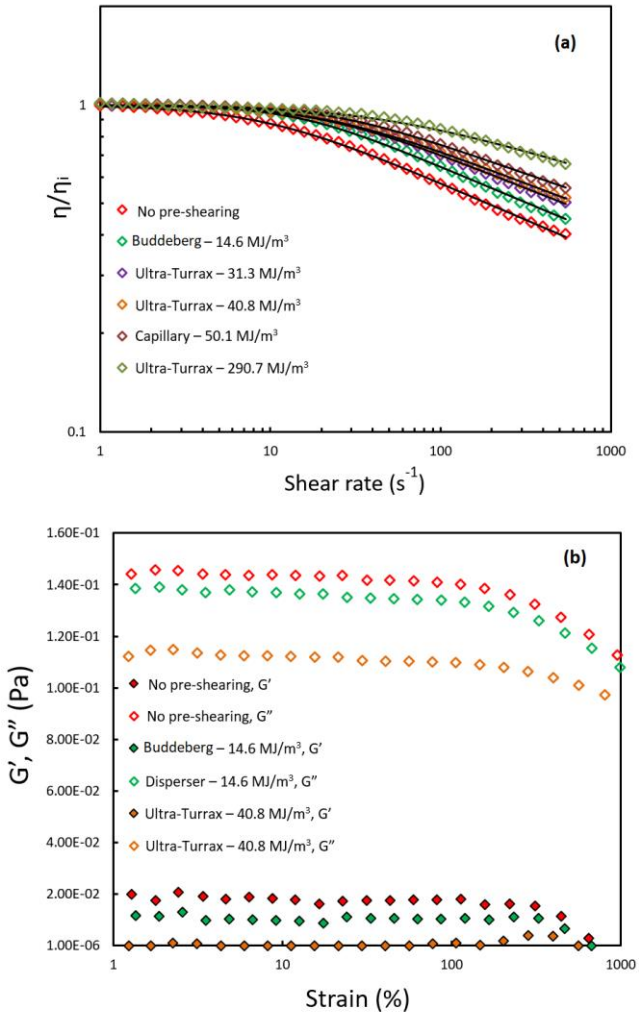

Figure 5. (a) The normalized steady-state shear viscosity of un- and pre-sheared polymer solutions. The solid line is acquired by fitting the experimental data into Carreau–Yasuda model. The fitting parameters are presented in Table S1 (see the supporting information). (b) The storage modulus (G') and loss modulus (G'') as a function of strain at constant angular frequency ω=6.28 rad/s

(RF) of the polymer solution. As a point of reference, RF will be compared at 30.0 ± 0.5 PV for all the experiments. Thereafter, the results of the numerical simulation will be presented to understand the behavior of polymer solutions flow through the sand-packs.

In Figure 6a, RFs of un-sheared and pre-shared polymer solutions are plotted as a function of the number of pore volumes (PV) forced through the sand-pack. When the un-sheared PS-A was forced through the sand pack, a significant increase in RF was observed, and only after 3.5 ± 0.5 PV injection of PS-A, the resistance factor rose to 30.0 ± 0.5. Thereafter, the rate of increase became slower and after 30.0 ± 0.5 PV, RF reached 84.5 ± 0.5.

Pre-shearing PS-A with Ultra-Turrax significantly enhanced the flow through the sand-pack. When Ultra-Turrax sheared PS-A at energy input of 31.3 MJ/m^3 was forced through the sand-pack for 30.0 ± 0.5 PV, RF rose

Table 4. Summary of performed sand-pack flow experiments

	Volume specific energy input (MJ/m^3)	Viscosity (mPa s)	Screen factor	Resistance factor at 30 PV
No pre-shearing	0	25.7	18.4	84.5
Ultra-Turrax	31.3	18.7	10.3	29.0
Ultra-Turrax	290.7	13.3	6.4	13.0

only to 29.0 ± 0.5 which represents a 66% decrease in RF compared to un-shared PS-A while the viscosity decreased only by 27%. Once the energy input of Ultra-Turrax significantly increased to 290.7 MJ/m^3, RF at 30.0 ± 0.5 PV dropped by an additional 19% whereas the viscosity dropped by an additional 21%. This reduction in RF of the pre-sheared polymer solutions is consistent with the reduction in SF formerly observed in the screen factor experiments.

Our results are in agreement with the study of Dupas et al.[48] who found that moderate mechanical degradation of HPAM prior to injection improves its injectivity in sand-packs. The authors found also that at high injection velocities, the apparent rheo-thickening for the degraded HPAM solution was less pronounced compared to the native HPAM solution which was attributed to the reduction of extensional viscosity at high degradation rates (i.e. rupture of longer chains) while the shear viscosity decreased only slightly.

A summary of parameters used in the numerical simulation to match the sand-pack flow experiments for each pre-shearing condition is given in Table S2. Figure 6a shows that the model was able to perfectly match the sand-pack flow experiments. A significant increase in RF of un-sheared PS-A at the beginning of the flow through the sand-pack is due to the combined effect of adsorption and mechanical entrapment leading to drastic polymer retention. Whether mechanical entrapment or adsorption is dominant depends on the permeability of the porous medium. Comparing the hydrodynamic radius of the polymer coil (R_h) and the pore throat radius (R_p), the adsorption may be the dominant mechanism for polymer retention in high-permeability sands ($R_p > 50R_h$)[49], while the mechanical entrapment dominates in low-permeability rocks ($R_p < 3R_h$).[14, 15, 49] Hence, the adsorption here is more dominant as the permeability of the sand-pack is relatively high. Nevertheless, after all the adsorption sites in the sand-pack are occupied with the polymer molecules, the mechanical entrapment becomes the dominant factor for polymer retention. Our model considers a time-dependent reduction in pore throat radius meaning that the pore throat becomes smaller due to the flow of many pore volumes of PS-A through the sand-pack and the consequent mechanical entrapment. As can be seen in Figure 6b, upon flowing PS-A through the sand-pack, the radius of pore throat becomes smaller and smaller. After 30.0 ± 0.5

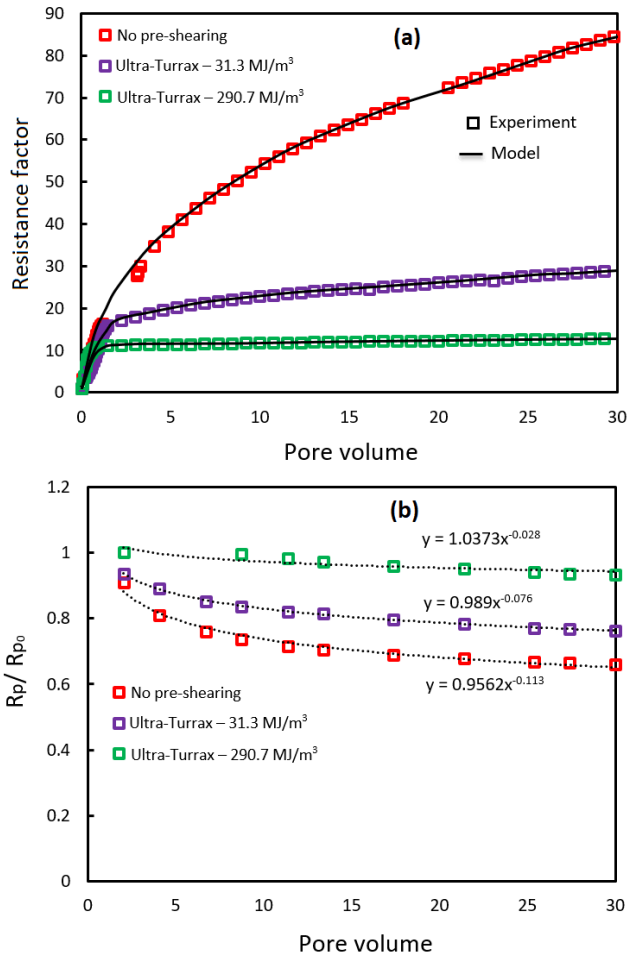

Figure 6. The sand-pack flow experimental and numerical modelling results. (a) Resistance factor (RF) as a function of pore volume for the flow of un-sheared and Ultra-Turrax sheared polymer solutions at different energy input through the sand-pack and (b) reduction in the radius of pore throat (R_p) as a function of pore volume

PV, 34% reduction in the radius of the pore throat is observed. This is consistent with a significant reduction in the size of polymer chains.

The flow of 30.0 ± 0.5 PV of Ultra-Turrax sheared PS-A at energy input of 31.3 MJ/m^3 through the sand-pack leads to a reduction of pore throat radius by 24% suggesting that the longest polymer chains have been broken after pre-shearing which makes the mechanical entrapment and continuous increase in RF less pronounced. The flow of 30.0 ± 0.5 PV of Ultra-Turrax sheared PS-A at energy input of 290.7 MJ/m^3 results in a decrease in pore throat radius only by 7% leading to a very gentle increase in RF. This is consistent with a significant reduction in the size of polymer chains.

Pre-shearing PS-A at high energy input of 290.7 MJ/m^3 leads to the best porous media flow enhancement. However, this is accompanied by a decrease in viscosity by 48%. This lower viscosity diminishes the ability of the polymer solution to improve the sweep efficiency and thus to enhance the oil recovery. Moreover, the significant energy applied to break the polymer chains is costly. Pre-shearing the polymer solution at the energy input of 31.3 MJ/m^3, however, results

in only a 27% reduction of viscosity while the applied energy is 90% reduced compared to the prior case. Therefore, there should be a trade-off between the flow enhancement, the viscosity reduction, and the cost of energy generation to choose the optimum level of energy input for pre-shearing the polymer solutions.

4. Conclusions

The effect of controlled pre-shearing by three shearing devices, namely a Buddeberg disperser, an Ultra-Turrax disperser, and pressure-driven flow through a capillary die on the flow of a polymer solution containing an inverse emulsion polymer dissolved in synthetic seawater was investigated. By comparing the flow properties of polymer solutions pre-sheared at different intensities, we conclude the following:

- A critical Weissenberg number was found (Wi_c~13) above which the viscosity of polymer solution started to decrease. The rate of viscosity reduction at large Wi became slower. Polymer pre-shearing was found to be path independent regardless of the shearing device.
- Plotting the viscosity and screen factor of pre-sheared polymer solution as a function of the energy dissipated by shearing devices resulted in establishing master curves. By increasing the energy input, first, only the screen factor decreased sharply while the reduction in viscosity was not as much. Later, both the screen factor and viscosity decreased significantly. These master curves for the polymer system were proven to be independent of the shearing device.
- Pre-shearing the polymer solution enhanced its flow efficiency in porous media. The Ultra-Turrax sheared polymer solution at the energy input of 31.3 and 290.7 MJ/m^3 showed a 66% and 85% drop in resistance factor respectively while the viscosity was reduced by 27% and 48% respectively.
- A numerical model for polymer flow in porous media accounting for time-dependent retention was built. Model predictions were found to be in good agreement with the reported experiments. The model assumed that the main mechanism for flow efficiency enhancement is a reduction in the size of polymer chains after pre-shearing which in turn leads to smaller mechanical entrapment and a less pronounced increase in resistance factor.
- The pre-shearing techniques can be applied to other polymers typically used for cEOR such as hydrolyzed polyacrylamide (HPAM) as shear degradation of HPAM (i.e. decrease in viscosity in shear flow fields) has also been reported in several studies.[50-54]
- Further studies are needed for determining the precise relationship between the shear and extensional flows as a result of pre-shearing. Moreover, direct measurements of MWD can better illustrate the concept of flow enhancement of water-soluble polymers in porous media. An extension of our study can be to investigate the effect of porous media permeability on the effectiveness of pre-shearing for flow enhancement particularly in low permeability cores where polymer injectivity is a serious challenge.

ASSOCIATED CONTENT

Supporting Information

The Supporting Information is available.
(1) Polymer injectivity, calculation of resistance factor and injectivity gradient; (2) calculation of shear rate and energy input; (3) calculation of strain rate for capillary; (4) molecular weight estimation of polymer; (5) Carreau–Yasuda model (Equation 1) for polymer viscosity model; (6) Numerical simulation parameters to match the sand-pack flow experiments; (7) Zero-shear rate viscosity estimation from Ubbelohde viscometer data

AUTHOR INFORMATION

Corresponding Author

Mohsen Mirzaie Yegane – Department of Geoscience and Engineering, Delft University of Technology, Stevinweg 1, 2628 CN Delft, The Netherlands; orcid.org/0000-0001-7060-4094; E-mail: M.mirzaieyegane@tudelft.nl, P.l.j.zitha@tudelft.nl

Notes

The authors declare no competing financial interest.

ACKNOWLEDGMENT

This study is the result of a collaboration between Delft University of Technology and TouGas Oilfield Solutions. We are grateful to TouGas Oilfield Solutions for permission to publish this work. Marita Neuber is greatly acknowledged for valuable comments and fruitful discussions.

REFERENCES

1. Paterson, R. W.; Abernathy, F. H., Turbulent flow drag reduction and degradation with dilute polymer solutions. *J. Fluid Mech* **1970,** 43, (4), 689-710.
2. Kang, K.; Lee, L. J.; Koelling, K. W., High shear microfluidics and its application in rheological measurement. *Exp Fluids* **2005,** 38, (2), 222-232.
3. Hu, X.; Boukany, P.; Hemminger, O.; Lee, L., The Use of Microfluidics in Rheology. *Macromol Mater Eng* **2011,** 296, 308-320.
4. Rems, L.; Kawale, D.; Lee, L. J.; Boukany, P. E., Flow of DNA in micro/nanofluidics: From fundamentals to applications. *Biomicrofluidics* **2016,** 10, (4), 043403-043403.
5. Banik, B. L.; Fattahi, P.; Brown, J. L., Polymeric nanoparticles: the future of nanomedicine. *WIREs Nanomed Nanobiotechnol* **2016,** 8, (2), 271-99.
6. El-Say, K. M.; El-Sawy, H. S., Polymeric nanoparticles: Promising platform for drug delivery. *Int J Pharm* **2017,** 528, (1-2), 675-691.
7. Nakamura, K., *Photopolymers: Photoresist materials, processes, and applications*; CRC Press, 2014; p 1-176.
8. Chen, Y., Nanofabrication by electron beam lithography and its applications: A review. *Microelectron Eng* **2015,** 135, 57-72.
9. Chauveteau, G., Fundamental Criteria in Polymer Flow Through Porous Media. In *Water-Soluble Polymers*, American Chemical Society: 1986; Vol. 213, pp 227-267.

10. Lake, L.W., Johns, R., Rossen, W., Pope, G., *Fundamentals of enhanced oil recovery*. Society of Petroleum Engineers: 2015.
11. Sorbie, K. S., *Polymer-Improved Oil Recovery*. Springer Netherlands: 1991.
12. Sheng, J., *Modern Chemical Enhanced Oil Recovery: Theory and Practice*. Gulf Professional Publishing: 2010.
13. Gogarty, W.B., Mobility Control With Polymer Solutions. *SPE J* **1967,** 7, (02), 161-173.
14. Szabo, M. T., Some Aspects of Polymer Retention in Porous Media Using a C14-Tagged Hydrolyzed Polyacrylamide. *SPE J* **1975,** 15, (04), 323-337.
15. Willhite, G. P.; Dominguez, J. G., MECHANISMS OF POLYMER RETENTION IN POROUS MEDIA. In *Improved Oil Recovery by Surfactant and Polymer Flooding*, Shah, D. O.; Schechter, R. S., Eds. Academic Press: 1977; pp 511-554.
16. Seright RS, M. J., Holzwarth G, Mechanical degradation of polyacrylamides induced by flow through porous-media. *ACS Polym. Prepr.* **1981,** 22, 30-33.
17. Beyer, M. K.; Clausen-Schaumann, H., Mechanochemistry: The Mechanical Activation of Covalent Bonds. *Chem. Rev.* **2005,** 105, (8), 2921-2948.
18. Gennes, P. G. D., Coil-stretch transition of dilute flexible polymers under ultrahigh velocity gradients. *J. Chem. Phys.* **1974,** 60, (12), 5030-5042.
19. Zimm, B. H., Dynamics of Polymer Molecules in Dilute Solution: Viscoelasticity, Flow Birefringence and Dielectric Loss. *J. Chem. Phys.* **1956,** 24, (2), 269-278.
20. Larson, R. G.; Magda, J. J., Coil-stretch transitions in mixed shear and extensional flows of dilute polymer solutions. *Macromolecules* **1989,** 22, (7), 3004-3010.
21. Perkins, T. T.; Smith, D. E.; Chu, S., Single Polymer Dynamics in an Elongational Flow. *Science* **1997,** 276, (5321), 2016.
22. Shaqfeh, E. S. G., The dynamics of single-molecule DNA in flow. *J Nonnewton Fluid Mech* **2005,** 130, (1), 1-28.
23. Sachdev, S.; Muralidharan, A.; Boukany, P. E., Molecular Processes Leading to "Necking" in Extensional Flow of Polymer Solutions: Using Microfluidics and Single DNA Imaging. *Macromolecules* **2016,** 49, (24), 9578-9585.
24. Odell, J. A.; Muller, A. J.; Narh, K. A.; Keller, A., Degradation of polymer solutions in extensional flows. *Macromolecules* **1990,** 23, (12), 3092-3103.
25. Giudice, F. D.; Haward, S. J.; Shen, A. Q., Relaxation time of dilute polymer solutions: A microfluidic approach. *J Rheol (N Y N Y)* **2017,** 61, (2), 327-337.
26. Nguyen, T. Q.; Kausch, H. H., Effects of solvent viscosity on polystyrene degradation in transient elongational flow. *Macromolecules* **1990,** 23, (24), 5137-5145.
27. Buchholz, B. A.; Zahn, J. M.; Kenward, M.; Slater, G. W.; Barron, A. E., Flow-induced chain scission as a physical route to narrowly distributed, high molar mass polymers. *Polymer* **2004,** 45, (4), 1223-1234.
28. Kuijpers, M. W. A.; Iedema, P. D.; Kemmere, M. F.; Keurentjes, J. T. F., The mechanism of cavitation-induced polymer scission; experimental and computational verification. *Polymer* **2004,** 45, (19), 6461-6467.
29. Sivalingam, G.; Agarwal, N.; Madras, G., Distributed midpoint chain scission in ultrasonic degradation of polymers. *AIChE J* **2004,** 50, (9), 2258-2265.
30. Jouenne, S.; Chakibi, H.; Levitt, D., Polymer Stability After Successive Mechanical-Degradation Events. *SPE J* **2018,** 23, (01), 18-33.
31. Müller, A. J.; Odell, J. A.; Carrington, S., Degradation of semidilute polymer solutions in elongational flows. *Polymer* **1992,** 33, (12), 2598-2604.
32. Garrepally, S.; Jouenne, S.; Olmsted, P.; Lequeux, F., *Scission of flexible polymers in contraction flow: predicting the effects of multiple passages*. *J Rheol (N Y N Y)* **2020,** 64, (3), 601-614.
33. Armanet, L.; Hunkeler, D., Phase inversion of polyacrylamide-based inverse-emulsions: Influence of inverting-surfactant type and concentration. *J. Appl. Polym. Sci* **2007,** 103, (6), 3567-3584.
34. González Rivera, J.; Hernández Barajas, J.; Gutiérrez Carrillo, A.; Aguilera Alvarado, A. F., Preparation of highly concentrated inverse emulsions of acrylamide-based anionic copolymers as efficient water rheological modifiers. *J. Appl. Polym. Sci.* **2016,** 133, (23).
35. Sorbie, K. S.; Roberts, L. J., A Model for Calculating Polymer Injectivity Including the Effects of Shear Degradation. In *SPE Enhanced Oil Recovery Symposium*, Society of Petroleum Engineers: Tulsa, Oklahoma, 1984; p 18.
36. Lim, T.; Uhl, J. T.; Prud'homme, R. K., The Interpretation of Screen-Factor Measurements. *SPE Res Eng* **1986,** 1, (03), 272-276.
37. Andrade, L. C. F.; Petronílio, J. A.; Maneschy, C. E. d. A.; Cruz, D. O. d. A., The carreau-yasuda fluids: a skin friction equation for turbulent flow in pipes and kolmogorov dissipative scales. *J. Braz.* **2007,** 29, 162-167.
38. Schmidt, J.; Mirzaie Yegane, M.; Dugonjic-Bilic, F.; Gerlach, B.; Zitha, P., Novel Method For Mitigating Injectivity Issues During Polymer Flooding at High Salinity Conditions. In *SPE Europec featured at 81st EAGE Conference and Exhibition*, Society of Petroleum Engineers: London, England, UK, 2019; p 17.
39. Yerramilli, S. S.; Zitha, P. L. J.; Yerramilli, R. C., Novel Insight into Polymer Injectivity for Polymer Flooding. In *SPE European Formation Damage Conference & Exhibition*, Society of Petroleum Engineers: Noordwijk, The Netherlands, 2013; p 23.
40. Hunkeler, D.; Nguyen, T. Q.; Kausch, H. H., Polymer solutions under elongational flow: 2. An evaluation of models of polymer dynamics for transient and stagnation point flows. *Polymer* **1996,** 37, (19), 4271-4281.
41. Vanapalli, S. A.; Islam, M. T.; Solomon, M. J., Scission-induced bounds on maximum polymer drag reduction in turbulent flow. *Phys. Fluids* **2005,** 17, (9), 095108.
42. Odell, J. A.; Keller, A., Flow-induced chain fracture of isolated linear macromolecules in solution. *J Polym Sci B Polym Phys* **1986,** 24, (9), 1889-1916.
43. Kamerkar, P. A.; Edwards, B. J., An experimental study of slip flow in capillaries and semihyperbolically converging dies. *Polym. Eng. Sci* **2007,** 47, (2), 159-167.
44. Hudson, N. E.; Jones, T. E. R., The Al project—an overview. *J Nonnewton Fluid Mech* **1993,** 46, (1), 69-88.
45. Walters, K., RECENT DEVELOPMENTS IN RHEOMETRY. In *Theoretical and Applied Rheology*,

Moldenaers, P.; Keunings, R., Eds. Elsevier: Amsterdam, 1992; pp 16-23.
46. Henaut, I.; Glenat, P.; Cassar, C.; Gainville, M.; Hamdi, K.; Pagnier, P., Mechanical Degradation Kinetics of Polymeric DRAs. In *8th North American Conference on Multiphase Technology*, BHR Group: Banff, Alberta, Canada, 2012; p 14.
47. Sánchez Pérez, J. A.; Rodríguez Porcel, E. M.; Casas López, J. L.; Fernández Sevilla, J. M.; Chisti, Y., Shear rate in stirred tank and bubble column bioreactors. *Chem. Eng. J* **2006,** 124, (1), 1-5.
48. Dupas, A.; Henaut, I.; Rousseau, D.; Poulain, P.; Tabary, R.; Argillier, J.-F.; Aubry, T., Impact of Polymer Mechanical Degradation on Shear and Extensional Viscosities: Toward Better Injectivity Forecasts in Polymer Flooding Operations. In *SPE International Symposium on Oilfield Chemistry*, Society of Petroleum Engineers: The Woodlands, Texas, USA, 2013; p 11.
49. Huh, C.; Lange, E. A.; Cannella, W. J., Polymer Retention in Porous Media. In *SPE/DOE Enhanced Oil Recovery Symposium*, Society of Petroleum Engineers: Tulsa, Oklahoma, 1990; p 20.
50. Díaz, F. A.; Torné, J. P.; Prada, A.; Perez, G., Shear degradation model of HPAM solutions for the design of regulator valves in polymer flooding EOR. *J Pet Explor Prod Technol* **2020,** 10, (6), 2587-2599.
51. Al-Shakry, B.; Skauge, T.; Shaker Shiran, B.; Skauge, A., Impact of Mechanical Degradation on Polymer Injectivity in Porous Media. *Polymers (Basel)* **2018,** 10, (7), 742.
52. Seright, R. S.; Seheult, J. M.; Talashek, T., Injectivity Characteristics of EOR Polymers. *SPE Reserv. Evaluation Eng.* **2009,** 12, (05), 783-792.
53. Driver, J. W.; Britton, C.; Hernandez, R.; Glushko, D.; Pope, G. A.; Delshad, M., Conditioning Polymer Solutions for Injection into Tight Reservoir Rocks. In *SPE Improved Oil Recovery Conference*, Society of Petroleum Engineers: Tulsa, Oklahoma, USA, 2018; p 10.
54. Al-Shakry, B.; Shiran, B. S.; Skauge, T.; Skauge, A., Enhanced Oil Recovery by Polymer Flooding: Optimizing Polymer Injectivity. In *SPE Kingdom of Saudi Arabia Annual Technical Symposium and Exhibition*, Society of Petroleum Engineers: Dammam, Saudi Arabia, 2018; p 22.

Table of Contents Graphic

The flow of pre-sheared water-soluble polymers in porous media is enhanced due to stretching the polymer chains (coil–stretch transition) and breaking the longest ones (rupturing the high-end fragments of the polymer molecular weight distribution).